

# Real-time simulation of finite-frequency noise from a single-electron emitter

T. Jonckheere,<sup>\*</sup> T. Stoll, J. Rech, and T. Martin*Centre de Physique Théorique, CNRS UMR 6207, Aix-Marseille Université, Case 907, F-13288 Marseille, France*

(Received 25 November 2011; revised manuscript received 9 January 2012; published 25 January 2012)

We study the real-time emission of single electrons from a quantum dot coupled to a one dimensional conductor, using exact diagonalization on a discrete tight-binding chain. We show that, from the calculation of the time evolution of the one-electron states, we have simple access to all the relevant physical quantities in the system. In particular, we are able to compute accurately the finite-frequency current autocorrelation noise. The method that we use is general and versatile, allowing us to study the impact of many different parameters, such as the dot transparency or level position. Our results can be directly compared with existing experiments, and can also serve as a basis for future calculations including electronic interactions using the time-dependent density-matrix renormalization group and other techniques based on tight-binding models.

DOI: [10.1103/PhysRevB.85.045321](https://doi.org/10.1103/PhysRevB.85.045321)

PACS number(s): 73.23.-b, 73.63.-b, 72.70.+m

## I. INTRODUCTION

The study of electronic transport in mesoscopic systems—where small size, low temperature, and careful fabrication of the sample ensure that quantum coherence is preserved—has shown tremendous progress in recent decades, providing a deep understanding of the behavior of these systems.<sup>1,2</sup> Recent progress opened the way to the study of these systems on short time scales, by looking at either the real-time dynamics or the high-frequency fluctuations.<sup>3–6</sup> A recent experiment has demonstrated the feasibility of single electron emission, where a single electron is periodically emitted from a quantum dot into an edge state of a two-dimensional (2D) electron gas in the quantum Hall effect regime<sup>7</sup> (see also Ref. 8). Measurements of the current and finite-frequency current correlations in this system confirmed that the system indeed behaves as a single-electron emitter.<sup>9</sup>

In this work, we study this system using real-time numerical simulations. Modeling the edge state and the quantum dot as a tight-binding chain without electronic interactions (see Fig. 1), we compute numerically the time evolution of the system when a time-dependent gate voltage is applied to the dot, using the time evolution of the one-electron states. We are able to study all the aspects of single-electron emission by calculating the average of all the relevant physical operators. In particular, we show that these real-time calculations allow us to compute accurately the finite-frequency autocorrelation noise of the emitted current, which has been used as definite experimental proof of single-electron emission.<sup>9</sup> In the optimal emission regime, our method provides very good agreement with the analytical results for the finite-frequency noise obtained from a semiclassical model,<sup>10</sup> which proves the power of real-time simulations in this context. More importantly, our approach

can be used to study several different regimes where no analytical results are available.

The goal of this work is twofold. First, as the single-electron emission experiments are currently performed in a regime where electronic interactions in the one-dimensional channel are small and can be neglected, the results obtained within our real-time simulation for noninteracting electrons are relevant, and can be directly compared with experimental data. We stress however that fermionic correlations are accounted for exactly with our approach. The method is quite versatile, and allows us to easily study the effect of various parameters, such as transparencies, temperature, the exact shape of the driving voltage, etc. Moreover, the real-time simulation gives us access to appealing visualisations of the electronic transport in these systems, with easy access to real-time density in real and energy space, as well as the shape of emitted wave packets. As a means to get results for the noninteracting system, our method thus appears to be complementary to calculations based on the Floquet scattering theory,<sup>11–15</sup> with equivalent results but different strengths and weaknesses.

Second, this work is a necessary first step toward the use of more involved real-time simulations, such as time-dependent density-matrix renormalization group (td-DMRG) and related techniques,<sup>16–23</sup> where electronic interactions can be taken into account in such a time-dependent situation.

The understanding of the role played by the different timescales, finite-size effects, and discretization, which our approach provides for noninteracting electrons, constitutes a prerequisite for the application of these more advanced and complex methods. In this regard, the present work is done in the same spirit as Ref. 24 (where shot-noise was computed from real-time dynamics) but actually goes beyond in considering the finite-frequency noise in a time-dependent setup.

This article is organized as follows. In Sec. II we detail the model we have used, and we derive expressions for the averages of physical quantities in terms of the numerical solution for the time evolution of the one-electron states. In Sec. III we present our results, first considering the static properties of the dot (mean charge), and then extending these considerations to the time-dependent properties (emitted charge density along the chain, emitted current, and autocorrelation noise). Section IV is devoted to discussions and conclusions.



FIG. 1. (Color online) Sketch of the system: a tight-binding chain of length  $L$ , with a dot defined on one end (red sites, at the right of the  $t_d$  link), on which a time-dependent potential  $V(t)$  is applied.

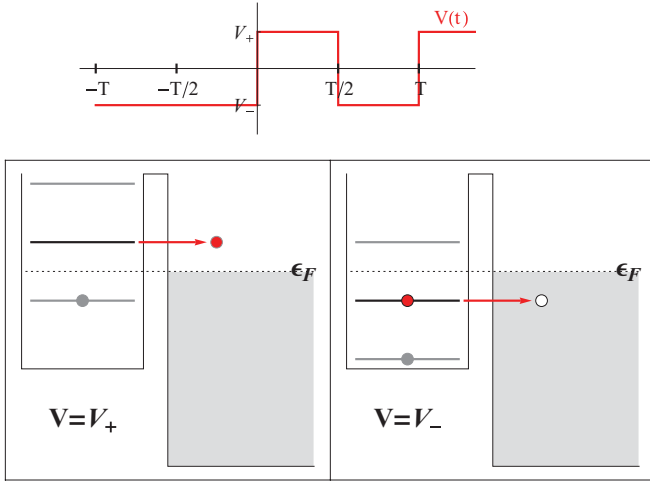


FIG. 2. (Color online) Top: Profile of the potential  $V(t)$  used in our calculations:  $V(t)$  is constant and equals  $V_-$  for  $t \leq 0$  (system in equilibrium), then shows perfect periodic steps between  $V_+$  and  $V_-$  for  $t > 0$ . Bottom: Illustration of the electron emission process in the optimal regime, where  $V_+ - V_- = \Delta$  (the level spacing of the dot), and the values of  $V_+$  and  $V_-$  are chosen such that the Fermi energy  $\epsilon_F$  of the chain is always in the middle of two energy levels. The left drawing shows the electron emission, when the driving potential brings an occupied level (black) above the Fermi energy; the right drawing shows the hole emission, when the empty level (black) is put below the Fermi energy by the driving potential.

## II. MODEL

### A. General formalism

The system is modeled as a one-dimensional (1D) tight-binding chain of length  $L$ , with the Hamiltonian

$$H = - \sum_{j=1, \neq j_d}^L (\hat{c}_j^\dagger \hat{c}_{j+1} + \text{H.c.}) - t_d (\hat{c}_{j_d}^\dagger \hat{c}_{j_d+1} + \text{H.c.}) + [\epsilon_d + V(t)] \sum_{j > j_d} \hat{c}_j^\dagger \hat{c}_j, \quad (1)$$

where  $\hat{c}_j$  and  $\hat{c}_j^\dagger$  are fermionic annihilation and creation operators at site  $j$ . The dot is composed of the sites  $j > j_d$ , with a tunneling amplitude  $t_d$  to or from the dot, an on-site energy  $\epsilon_d$ , and an applied time-dependent potential  $V(t)$ . To perform periodic single-electron emission,  $V(t)$  is a periodic function of time (with period  $T$ ), which in the optimal situation brings alternatively the highest occupied dot level above the Fermi energy in the leads (electron emission), and the lowest unoccupied state below the Fermi energy (hole emission); see Fig. 2. In order to compute the evolution of the system, we consider it to be in equilibrium at  $t \leq 0$  with  $V(t) = \text{const}$ , while the periodic potential is applied for  $t > 0$ .

For  $t \leq 0$ , the system is in equilibrium, and we can compute the  $L$  eigenstates of the Hamiltonian  $H$ , denoted  $\phi_i$  ( $i = 1, \dots, L$ ) with increasing energies  $E_1 < E_2 < \dots < E_L$ . The initial  $N$ -particle state, at zero temperature, is simply obtained by filling the  $N$  lowest energy states. For nonzero temperature, the occupation of the states is given by the Fermi distribution. In the following, we will work with the chain at half-filling, with  $N = L/2$ . For  $t > 0$ , the evolution of

each one-electron states  $\phi_i(t)$  can be obtained by solving the time-dependent Schrödinger equation

$$i\hbar \frac{\partial \phi_i(t)}{\partial t} = H(t) \phi_i(t). \quad (2)$$

This can be achieved by numerical integration of the differential equation for an arbitrary potential  $V(t)$ .

As there are no electronic interaction in the system, each occupied electronic state evolves independently from the other states, and the  $N$ -particle state at time  $t > 0$  is simply obtained by filling the same one-electron state as for the initial state, but using now the time-dependent  $\phi_i(t)$ . Introducing  $\hat{\phi}_i^\dagger(t)$  as the fermionic operator creating an electron in the single-electron state  $i$  at time  $t$ , the  $N$ -particle wave function of the chain at time  $t$  is

$$|\Psi(t)\rangle = \hat{\phi}_1^\dagger(t) \hat{\phi}_2^\dagger(t) \cdots \hat{\phi}_{L/2}^\dagger(t) |0\rangle \equiv |1, 1, \dots, 1, 0, 0, \dots, 0\rangle_t, \quad (3)$$

where  $|0\rangle$  denotes the empty band.

We want to stress that this method does not rely on any adiabatic approximation for the evolution due to  $V(t)$ , and it can be applied with an arbitrary potential  $V(t)$ . In a nutshell, what we are doing is simply taking the system in a given initial state ( $t < 0$ ), and computing its time evolution using the time-dependent Schrödinger equation. This can be done in principle for any system (e.g., even with electronic interactions), but would be impractical at the level of the  $N$ -electron state because of the huge size of the Hilbert space. But since we are considering here noninteracting electrons, this can be done for each electron independently [Eq. (2)], thus relatively easily.

For the sake of simplicity, we consider here the special case of a piecewise constant potential  $V(t)$ , which allows us to reduce the numerical integration of the differential equation to simple matrix products (see below). Note however that the numerical cost of solving numerically the differential equation with a more complex  $V(t)$  is only slightly higher, so in practice our method can be applied without difficulty to any reasonable form of  $V(t)$ . We thus focus on a potential  $V(t)$  which at  $t > 0$  consists of perfect periodic steps (see Fig. 2) and takes the form

$$V(t) = \begin{cases} V_- & \text{if } t \leq 0, \\ V_+ & \text{if } 0 + nT \leq t < \frac{T}{2} + nT, \\ V_- & \text{if } \frac{T}{2} + nT < t \leq T + nT, \end{cases} \quad (4)$$

where  $n$  is a positive integer. In this case, knowing the eigenvalues and eigenstates of the system for  $V = V_-$  and  $V = V_+$  is enough to get the time evolution of any one-particle state by expressing it alternatively in the basis of these eigenstates. During a time interval where  $V(t)$  is constant, the time evolution is simply given by phase factors coming from the eigenenergies. Then the sudden switch of  $V(t)$  from  $V_+$  to  $V_-$  (or vice versa) is accounted for by a basis transformation from the  $V_+$  eigenstates to the  $V_-$  eigenstates (or vice versa), which ultimately amounts to a simple matrix product. By combining the trivial time evolution for a constant  $V(t)$  with the change of basis when  $V(t)$  switches from one value to another, we easily get access to the one-particle state evolution for any time  $t$ .

### B. Calculation of operator average

The fermionic operator for the one-particle state  $\hat{\phi}_i(t)$  can be written in full generality in the basis of the position states along the chain:

$$\hat{\phi}_i(t) = \sum_{j=1}^L \alpha_{i,j}(t) \hat{c}_j, \quad (5)$$

where  $\alpha_{i,j}(t)$  is a time-dependent unitary matrix. This matrix is the natural object coming out of the numerical evolution of the system, as it expresses the one-particle states at time  $t$  in terms of the position states. In particular, the lines of the matrix  $\alpha_{i,j}(t)$  at  $t = 0$  correspond to the eigenstates of the Hamiltonian (1), which are naturally obtained in the position-state basis, as is the Hamiltonian itself.

For convenience, we compute all the operator averages in the Heisenberg picture. The time-dependent position operators along the chain can then be written as

$$\hat{c}_k(t) = \sum_{m=1}^L \alpha_{m,k}^*(t) \hat{\phi}_m(0), \quad (6)$$

where the one-electron states operators are taken at  $t = 0$ .

#### 1. Average current

The current operator on link  $k$  (between sites  $k$  and  $k + 1$ ) at time  $t$  is

$$\hat{I}_k(t) = -i(\hat{c}_k^\dagger(t) \hat{c}_{k+1}(t) - \text{H.c.}) \quad (7)$$

and its average is

$$\begin{aligned} \langle I_k(t) \rangle = & -i \left( \sum_{m,n} \alpha_{m,k}(t) \alpha_{n,k+1}^*(t) \right. \\ & \left. \times \langle \Psi(0) | \hat{\phi}_m^\dagger(0) \hat{\phi}_n(0) | \Psi(0) \rangle - \text{H.c.} \right) \end{aligned} \quad (8)$$

with  $|\Psi(0)\rangle \equiv |\Psi\rangle$ , the half-filled Fermi sea at time  $t = 0$ . Using Eq. (3), at zero temperature the average of the  $\hat{\phi}$  operator product is simply  $\delta_{m,n}$  for the occupied states ( $m \leq L/2$ ), and 0 for the empty ones ( $m > L/2$ ), leading to

$$\langle I_k(t) \rangle = 2 \sum_{n \leq L/2} \text{Im}[\alpha_{n,k}(t) \alpha_{n,k+1}^*(t)]. \quad (9)$$

At nonzero temperature, one has  $\langle \hat{\phi}_n^\dagger \hat{\phi}_n \rangle = f(E_n)$ , where  $f(E)$  is the Fermi function at energy  $E$ , and the average current becomes

$$\langle I_k(t) \rangle = 2 \sum_{n=1}^L f(E_n) \text{Im}[\alpha_{n,k}(t) \alpha_{n,k+1}^*(t)]. \quad (10)$$

#### 2. Current correlations

The correlation between the current at link  $k$  and time  $t_1$  with the one at link  $l$  and time  $t_2$  is given by

$$S_{k,l}(t_1, t_2) = \langle \Psi | I_k(t_1) I_l(t_2) | \Psi \rangle - \langle \Psi | I_k(t_1) | \Psi \rangle \langle \Psi | I_l(t_2) | \Psi \rangle. \quad (11)$$

Proceeding along the same lines as for the current average, and using Wick's theorem for averages involving four  $\hat{\phi}$  operators, we get at finite temperature

$$\begin{aligned} S_{k,l}(t_1, t_2) = & (-1) \sum_{m=1}^L \sum_{n=1}^L f(E_m) [1 - f(E_n)] \\ & \times [\alpha_{m,k}(t_1) \alpha_{n,k+1}^*(t_1) - \alpha_{m,k+1}(t_1) \alpha_{n,k}^*(t_1)] \\ & \times [\alpha_{n,l}(t_2) \alpha_{m,l+1}^*(t_2) - \alpha_{n,l+1}(t_2) \alpha_{m,l}^*(t_2)]. \end{aligned} \quad (12)$$

### 3. Mean charge on the dot

The operator  $\hat{Q}(t)$  describing the charge on the dot is

$$\hat{Q}(t) = \sum_{j>jd} \hat{c}_j^\dagger(t) \hat{c}_j(t), \quad (13)$$

leading to the average charge

$$\begin{aligned} \langle Q(t) \rangle = & \sum_{j>jd} \sum_{m,n} \alpha_{m,j}(t) \alpha_{n,j}^*(t) \langle \Psi(0) | \hat{\phi}_m^\dagger(0) \hat{\phi}_n(0) | \Psi(0) \rangle \\ = & \sum_{j>jd} \sum_{n=1}^L f(E_n) |\alpha_{n,j}(t)|^2. \end{aligned} \quad (14)$$

The results from Eqs. (10), (12), and (14) show that all the averages can easily be computed from the time-dependent matrix  $\alpha_{i,j}(t)$ , which is directly obtained from the numerical computation of the time evolution.

## III. RESULTS

### A. Parameters and operating regime

We present below the results that we have obtained to characterize the emission of single electrons in the one-dimensional chain. One must be aware that our approach uses a nonchiral system, where excitations can propagate to the left and to the right, in order to simulate a chiral system (an edge state of the quantum Hall effect). In our setup, the left-going excitations correspond to the ones coming out of the dot in the real system, while the right-going excitations are incoming onto the dot, and thus need to be avoided. Multiple reflections inside the simulated dot are equivalent in the real system to performing multiple round trips inside the dot.

In the remainder of the text, we work with a dot composed of five sites, located at the end of a much longer chain (approximately a few hundred sites, typically 500). This size of the dot is the result of a compromise. On the one hand, the dot has to be as small as possible compared to the chain, in order to minimize finite-size effects. Indeed the level spacing in the chain must be negligible compared to the level spacing in the dot, in order to appear as a continuum. On the other hand, since we apply a time-dependent voltage of the order of the dot level spacing, the latter needs to be small compared to the bandwidth of the tight-binding chain, in order to minimize the effects of the nonlinear dispersion relation of the chain. As the level spacing is inversely proportional to the size of the dot, one thus needs to consider a large enough dot to meet this requirement. In practice, we found that using a dot of five sites was a good compromise, in particular because we were able to perform the current measurement near the dot, thus

reducing the spreading of wave packets during propagation, which arises from the nonlinear dispersion.

We consider the chain to be at half-filling, and work with physical dimensions corresponding to  $\hbar = e = 1$ . The tunneling amplitude along the chain [first term in the Hamiltonian (1)] has been taken as the unit of energy, and as a consequence the Fermi velocity at half-filling is equal to 2 sites per unit of time. This means that an excitation takes a time  $L$  to reflect at the boundary and come back to its starting point along a chain of  $L$  sites. In particular, the current measured at a given link due to the passage of an excitation will be completely spoiled after a time  $L$  by the reflection of that same excitation at the end of the chain. One can thus expect that the numerical quantities we compute will be reliable up to a time  $\sim L$  only.

Unless specifically stated, all the results presented below were obtained in the optimal regime for electron emission. In this regime, the amplitude of the driving potential,  $V_+ - V_-$ , is taken to be equal to the dot level spacing  $\Delta$ . When the driving potential switches to the value  $V_+$ , one energy level of the dot is put at an energy  $\epsilon_F + \Delta/2$  (where  $\epsilon_F$  is the Fermi energy of the chain), and an electron is emitted at this very energy (see the bottom left panel of Fig. 2). When  $V(t)$  switches back to  $V_-$ , this same level is brought down to the energy  $\epsilon_F - \Delta/2$ , and a hole is emitted, i.e., an electron tunnels back to the dot level (see the bottom right panel of Fig. 2). This parameter regime is the one best suited to emit a true single electron and a single hole during each period, as has been shown experimentally,<sup>7</sup> and it is thus the most relevant one for our study. Note however that there is no difficulty in exploring other operating regimes with our method (for example, a dot level in resonance with  $\epsilon_F$ ).

### B. Static properties of the dot

Before studying the properties of the electron emission by the dot, it is necessary to characterize the properties of the dot itself without a time-dependent potential  $V(t)$  applied. Figure 3 shows the mean charge on the dot as a function of the on-site energy  $\epsilon_d$ , for several values of the tunneling amplitudes to the dot  $t_d$  at zero temperature (top plot), and for increasing temperature with  $t_d = 0.2$  (bottom plot). For a small value of  $t_d$  at zero temperature, we observe that the mean charge is quantized, with well defined plateaus at integer value. This simply reflects that when the dot is weakly coupled to the chain, the number of electrons on the dot is an integer: it can vary between 5 and 0, leading to five energy levels. Indeed, the density of states (not shown) that corresponds to  $\partial\langle Q\rangle/\partial\epsilon_F = -\partial\langle Q\rangle/\partial\epsilon_d$  has five narrow peaks at the position of the steps in  $\langle Q\rangle$ , corresponding to the five energy levels of the dot. As  $t_d$  is increased, the steps between the plateaus are smoothed due to the increased fluctuations between the dot and the chain, leading to broadened energy levels. Increasing the temperature for fixed  $t_d$  (bottom plot) has a similar effect: it broadens the energy levels, leading to smoothed steps.

For the parameters we have chosen, the level spacing of the dot  $\Delta$  is of the order of 1. Yet, because of finite-size effects, the level spacing  $\Delta$  is not constant and depends on the levels considered. We thus focus on the electron and hole emission from the central level of the dot ( $\epsilon_d = 0$ ), for which the optimal emission regime is obtained by taking  $V_+ = -V_- \simeq 0.6$ .

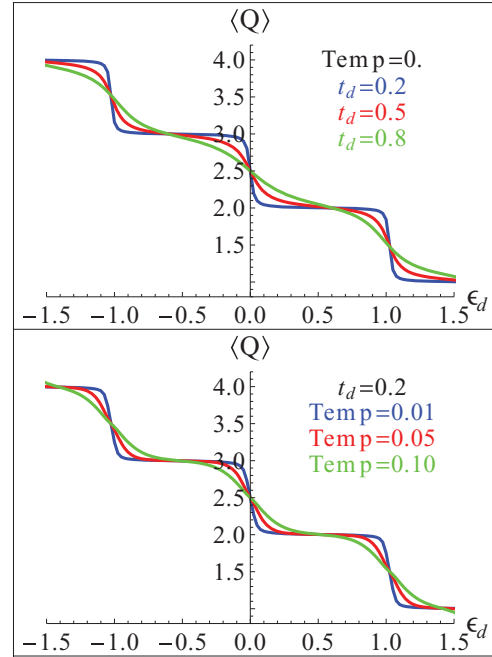


FIG. 3. (Color online) Mean charge on the dot as a function of the on-site energy of the dot  $\epsilon_d$ , for several tunneling amplitudes to the dot  $t_d$  at zero temperature (top), and for several temperatures at  $t_d = 0.2$  (bottom). For small  $t_d$  and temperature, the mean charge tends to be quantized at integer values, with sharp steps between the plateaus. When  $t_d$  or the temperature are increased, the steps are smoothed due to the increased fluctuations between the dot and the lead.

### C. Time-dependent charge on the dot

We consider now the time-dependent charge on the dot when  $V(t)$  is applied, in the optimal emission regime ( $\epsilon_d = 0$ ,  $V_+ = -V_- = 0.6$ ). Figure 4 shows the mean charge for this choice of  $V_+, V_-$  as a function of time ( $0 < t < T$ ), for several values of the tunneling amplitude to the dot  $t_d$ , at zero temperature. Several observations can be made from these plots.

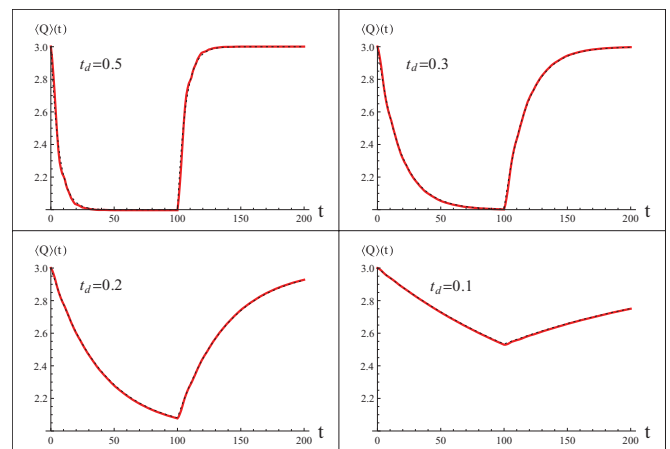


FIG. 4. (Color online) Mean charge  $\langle Q \rangle$  on the dot as a function of time when  $V(t)$  is applied for different tunneling to the dot  $t_d$  at zero temperature. This data is obtained for a chain of length  $L = 500$ , with a period  $T = 200$ .

First, when the potential  $V$  is switched from  $V_-$  to  $V_+$  (at  $t = 0$ ), one electron leaves the dot, and the charge, up to a very good approximation, decreases exponentially,

$$\langle Q \rangle(t) \simeq 2 + \exp(-t/\tau), \quad (15)$$

with a characteristic time  $\tau$  which increases as  $t_d$  decreases. Calculations in the continuous limit for a perfect dot predict<sup>7</sup>

$$\tau \simeq \frac{2\pi}{\Delta} \frac{1}{D}, \quad D \ll 1, \quad (16)$$

where  $D$  is the transparency of the dot. For the tight-binding chain that we consider, the relation between the tunneling amplitude  $t_d$  and the transparency is, in the linear regime of voltage,<sup>25–27</sup>

$$D(t_d) \simeq \frac{4t_d^2}{(1 + t_d^2)^2}. \quad (17)$$

Using this expression of  $D(t_d)$  and performing a fit of the data gives the function  $\tau \simeq 6.1/D(t_d)$ , with a reasonable agreement with the value of the level spacing in our system ( $6.1 \simeq 2\pi/\Delta$  for  $\Delta \simeq 1$ ).

When the potential  $V(t)$  switches back to  $V_-$  (for  $t \geq T/2$ ), the charge starts to increase (as an electron comes back inside the dot, or equivalently a hole comes out of the dot), and the behavior is symmetrically reversed, with a similar exponential growth back toward the initial charge.

Second, the qualitative behavior of the system changes as the ratio of the decay time  $\tau$  to the half-period  $T/2$  changes. When  $\tau \ll T/2$ , the electron is emitted/absorbed from the dot much faster than the half-period, and the emitted/absorbed charge is close to 1. This is the case on the two upper plots of Fig. 4, where it is clear that the charge  $\langle Q \rangle$  goes all the way from 3 to 2 on the first half-period, then back from 2 to 3 on the second half-period. The electron is thus emitted or absorbed with a probability close to 1 at each half-period. On the other hand, when  $\tau > T/2$ , the electron emission/absorption is not complete during one half-period, which means that the probability that an electron is emitted or absorbed on each half-period is smaller than one. This is shown on the bottom plots of Fig. 4.

Note that, in this regime ( $\tau > T/2$ ), the variation of the charge during one half-period is smaller than 1. One has then to be careful with the choice of initial conditions. Indeed, we are trying to model a periodic system using a finite one starting from an equilibrium or ground-state configuration. Depending on the initial parameters, the system will take one or several periods to relax toward the permanent periodic regime (which is independent of the initial conditions). This is illustrated on the left plot of Fig. 5, which shows  $\langle Q \rangle(t)$ , with  $\tau \gg T/2$ , for several periods (we chose  $T = 50$  for a chain of length  $L = 1000$ , to be able to compute the evolution on many periods without suffering from reflections at the boundary of the chain). It is clear that the extrema of the oscillations of  $\langle Q \rangle$  tend to relax toward long-term values  $2 + Q_+$  and  $2 + Q_-$ . As it is numerically very inefficient to compute the evolution over many periods (it requires very long chains to avoid boundary effects), we have to modify the initial conditions in order to reach the periodic regime as soon as the time-dependent potential is applied. Knowing the value of the escape time  $\tau$  from the dot for our choice of parameters,

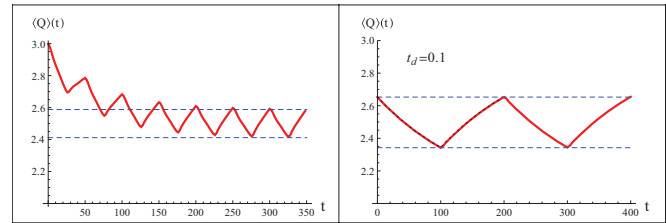


FIG. 5. (Color online) Mean charge  $\langle Q \rangle$  on the dot as a function of time when  $V(t)$  is applied, in the regime where  $\tau \gg T/2$  (small tunneling amplitude to the dot). The left plot, obtained with a period  $T = 50$  on a chain of length  $L = 1000$ , shows that starting at  $t = 0$  with  $\langle Q \rangle = 3$  does not correspond to the long-time limit: after several periods one reaches a long-time regime where  $\langle Q \rangle$  oscillates between the values  $2 + Q_+$  and  $2 + Q_-$ . The right plot, obtained with a period  $T = 200$  on a chain of length  $L = 500$ , shows that it is possible to access the long-time limit from  $t = 0$  by switching on  $V(t)$  at an earlier time  $t_{in} < 0$  to get the correct charge  $\langle Q \rangle(t = 0) = 2 + Q_+$  (see text for details).

and introducing  $s = \exp(-\frac{T}{2\tau})$ , the values of  $Q_+$  and  $Q_-$  can be predicted analytically by solving the equations expressing that the charge at the end of one period (at  $t = nT + T - 0$ ) has to be the same as the charge at the beginning of the period (at  $t = nT + 0$ ):

$$Q_- = s Q_+, \quad Q_+ = s Q_- + (1 - s), \quad (18)$$

giving  $Q_+ = 1/(1 + s)$  and  $Q_- = s/(1 + s)$ . In practice, in order to have the correct value of the charge ( $2 + Q_+$ ) at  $t = 0$ , we switch the potential  $V(t)$  from  $V_-$  to  $V_+$  at a time  $t_{in} < 0$ , such that the value of  $\langle Q \rangle$  at time  $t = 0$  is precisely  $2 + Q_+$ . We are thus letting a fraction of electrons escape from the dot for  $t < 0$ , in order for the charge to take the right value at  $t = 0$ . The result of this procedure is shown on the right plot of Fig. 5. One can see that the charge has indeed the predicted periodic behavior, with increase and decrease between the values  $2 + Q_+$  and  $2 + Q_-$  shown as dashed lines.

#### D. Visualization of the time-dependent density

The numerical results allow us to obtain a visual representation of the emitted wave packets propagating along the chain. The left part of Fig. 6 shows an example of the results, obtained for a chain of length  $L = 500$ , and an intermediate value for the dot tunneling amplitude,  $t_d = 0.4$ , at zero temperature. The chain is initially in equilibrium at half-filling (occupation = 0.5 on all sites, except on the dot at the extreme right of the chain, which contains three electrons). Starting at  $t = 0$ , the electron is emitted and appears as a left-propagating wave packet, which initially has an exponential profile. As it propagates along the chain, this wave packet broadens due to the nonlinear spectrum of the chain. At  $t = 100 = T/2$  the emission of a hole starts, with properties similar to the electron.

Performing a Fourier transform for each of the one-electron states gives us access to the density in the wave-vector space (or  $k$  space) as a function of time, which is shown on the right part of Fig. 6. Initially, the system is in equilibrium, at zero temperature, and has all the states for  $|k| < k_{max}$  occupied (occupation 1, the “Fermi sea”) while all the other states are empty. For  $t > 0$ , the electron emission shows up as a well

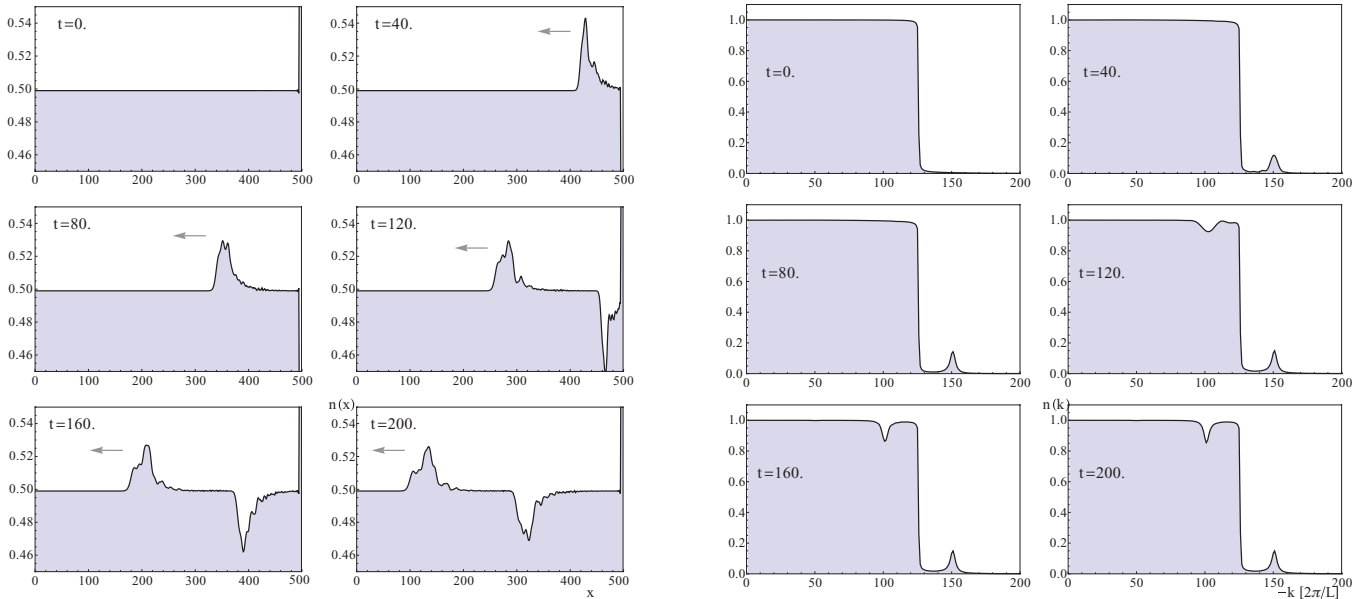


FIG. 6. (Color online) (Left) Density along the chain (mean occupation of each site) at different times for a chain of length  $L = 500$ , with a dot tunneling amplitude  $t_d = 0.4$ , at zero temperature, over one period of length  $T = 200$ . One clearly sees the emission of the electron at  $t = 0$  with an exponential profile, and of a hole at  $t = T/2 = 100$ . Because of the nonlinear spectrum of the chain, wave packets broaden during propagation. (Right) Same evolution shown for the occupation in  $k$  space, for negative  $k$  (left-going excitation). The emission of the electron shows up as a well defined peak above the occupied states.

defined peak above the Fermi sea. Similarly, the emission of the hole for  $t > 100$  appears as a dip in the Fermi sea. Both structures manifest at the same distance from  $k_F$ , confirming that the electron and hole are emitted with energies symmetric with respect to the Fermi level.

Looking at the density in  $k$  space for different tunneling amplitudes  $t_d$  gives us information about the properties of the emitted electron, and about the “quality” of the electron emission. Figure 7 shows the electron peak for a small tunneling amplitude  $t_d = 0.2$  and a larger one  $t_d = 0.6$  (and other parameters as in Fig. 6). A small transparency leads to a narrow peak that is well separated from the Fermi sea, while a larger transparency creates a broader peak that tends to merge with the Fermi sea.<sup>14</sup>

### E. Time-dependent current

The current coming out of the dot contains information similar to the time-dependent charge on the dot, as it is given

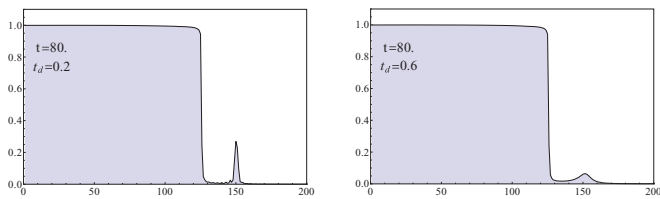


FIG. 7. (Color online) Effect of the dot tunneling amplitude  $t_d$  on the electron peak in momentum space, for  $t_d = 0.2$  (left) and  $t_d = 0.6$  (right), for a chain of 500 sites, with other parameters as in Fig. 6. A smaller transparency leads to a narrower peak, well separated from the occupied states, while a larger transparency gives a broader peak which tends to merge with the occupied states.

by the time derivative of this charge. We recall that the current is computed on a link very close to the dot (a few sites away), in order to minimize the effect of the nonlinear spectrum of the chain, which tends to spread the wave packet propagating along the chain during its travel.

Figure 8 shows the current for the same parameters as in Fig. 4, computed from Eq. (9) between sites 490 and 491 for a chain of length 500. For  $t_d = 0.5$  and  $0.3$ , the current shows a dip followed by a peak, due to the passage of the electron then the hole. The peaks have an exponential profile with some oscillations that correspond to the ones present in the charge  $\langle Q \rangle(t)$  [we could check explicitly that computing

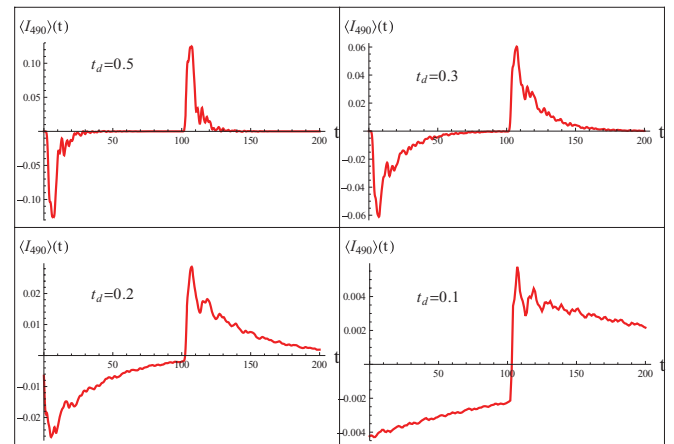


FIG. 8. (Color online) Mean current  $\langle I \rangle$  between sites 490 and 491 as a function of time when  $V(t)$  is applied for different tunneling to the dot  $t_d$  at zero temperature. Data obtained for a chain of length  $L = 500$ , with a period  $T = 200$ .

$d\langle Q\rangle(t)/dt$  gives the same peaks]. As  $t_d$  is reduced, the width of the electron and hole wave packets increases, and becomes larger than the half-period. This is apparent on the plots for  $t_d = 0.2$  and  $t_d = 0.1$ , where the current does not reach zero at  $t = 100 = T/2$ . There, when the external drive switches from  $V_+$  to  $V_-$  and the hole emission begins, the sign of the current changes abruptly. Bear in mind that we had to start the emission at time  $t_{in} < 0$  (see Sec. III C) in order to be immediately in the periodic regime at  $t = 0$ . This has the undesired consequence of reducing the oscillations of the current in the first half-period compared to the following ones, as can be seen on the bottom right plot of Fig. 8 (the current for later periods—not shown—is similar to the one of the second half-period). This is because, when using a nonzero  $t_{in}$ , the charge has the correct “periodic” value at  $t = 0$ , but there is no abrupt change of the potential at that time, unlike what happens at  $t = T/2, T, \dots$ . The values for the current during the first half-period are thus somewhat inaccurate. For this reason, in the calculation of the current autocorrelations (see below), we use the current starting from the second half-period only.

### F. Current autocorrelations

The current correlations at finite frequency contain more information about the single-emission process than the mean current or the mean charge do.

We have computed the autocorrelation for currents on the same link,

$$S_{k,k}(t_1, t_2) = \langle \Psi | I_k(t_1) I_k(t_2) | \Psi \rangle - \langle \Psi | I_k(t_1) | \Psi \rangle \langle \Psi | I_k(t_2) | \Psi \rangle, \quad (19)$$

for a link  $k$  close to the dot. Because the applied voltage is periodic in time,  $S_{k,k}(t_1, t_2)$  is a periodic function of the mean time  $(t_1 + t_2)/2$ . By taking the average over one period  $T$ , we obtain the autocorrelation noise, which depends on the time difference only:

$$S_{k,k}(t) = \overline{S_{k,k}(t', t' + t)}. \quad (20)$$

Performing a Fourier transform of  $S_{k,k}(t)$  gives access to the autocorrelation noise as a function of frequency. This quantity has been measured experimentally for a frequency of the order of the frequency of the applied voltage  $V(t)$ , as reported in Ref. 9. Using a semiclassical model, valid in the optimal emission regime where the Fermi energy of the chain is halfway between two dot levels, Albert *et al.*<sup>10</sup> have provided an analytical formula for the autocorrelation noise as a function of the frequency  $\omega$  and the escape time  $\tau$  of the electron from the dot:

$$S_{k,k}(\omega) = \frac{2}{T} \tanh\left(\frac{T}{4\tau}\right) \frac{\omega^2 \tau^2}{1 + \omega^2 \tau^2}, \quad (21)$$

where  $T$  is the period of the applied voltage. A good agreement between this formula and the experimental results was obtained.<sup>9,10</sup>

Figure 9 shows the results obtained for  $S_{k,k}(\omega = 2\pi/T)$  in units of the driving frequency ( $1/T$ ), as a function of the escape time of the dot scaled by the half-period  $\tau/(T/2)$ , for a chain of length  $L = 600$  with a period  $T = 200$ . The current correlations were computed at zero temperature, close to the

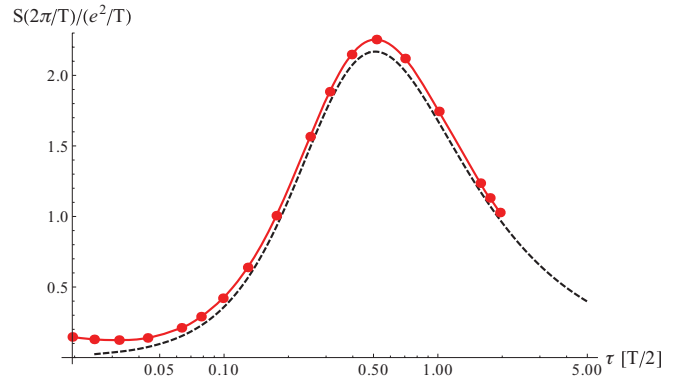


FIG. 9. (Color online) Autocorrelation noise  $S$  of the current on link 590, taken at the frequency  $2\pi/T$  of the applied potential  $V(t)$ , as a function of the escape time from the dot. The noise is expressed in units of the drive frequency ( $1/T$ ), while the escape time is in units of the half-period ( $T/2$ ). The black dashed curve shows the theoretical prediction of the semiclassical model of Ref. 10. The red points show the results obtained with our calculations, for a chain of length  $L = 600$  and a period  $T = 200$ .

dot, on the link between sites 590 and 591 (while the dot occupies sites 596 to 600). Note that in this regime, the results are nearly insensitive to temperature, as long as it is much smaller than the level spacing in the dot. The first observation to be made is that the numerical results (red points) are very close to the predicted analytical formula (dashed black curve); the numerical curve is just slightly above the theoretical one (by  $\approx 4\%$ ).

The curve has a maximum for  $\tau \sim T/2$ , delimiting two regions that correspond to two different regimes. On the left of the maximum, when  $\tau \ll T/2$ , the emission time of the electron or hole is much shorter than the half-period, so it is emitted with probability 1, and the noise comes from the uncertainty in the emission time, which decreases with  $\tau$ . This is the jitter regime, or phase-noise regime. On the right, when  $\tau \gg T/2$ , the emission time of the electron or hole is larger than the half-period, so the emission probability is smaller than 1, which is the cause of the noise. This is thus the shot-noise regime, or charge-noise regime. Note that the deviations of our numerical results with respect to the theoretical curve are similar in both regimes. This is a good indication of the reliability of our calculations, in particular that the use of an initial time  $t_{in} < 0$ , which is only needed in the shot-noise regime (see Sec. III C), gives correct results. Larger deviations appear only for very small values of  $\tau/(T/2)$ , which correspond to the large transparency regime when the escape time from the dot gets close to the time of a round trip inside the dot. The semiclassical model cannot be used in that regime and the analytical formula (21) is no longer valid.

We have chosen the period  $T = 200$  to be as large as possible for the chain length  $L = 600$ , taking into account the finite size constraints. Indeed, the maximum time before an emitted wave packet is reflected at the boundary of the chain and comes back, spoiling the measurement of the current, is approximately  $t_{\max} \simeq 600$  (because the Fermi velocity is 2 sites per unit of time). The time averaging procedure [Eq. (20)] requires at least one period  $T$ , while the integration for the Fourier transform needs at least another period  $T$ .

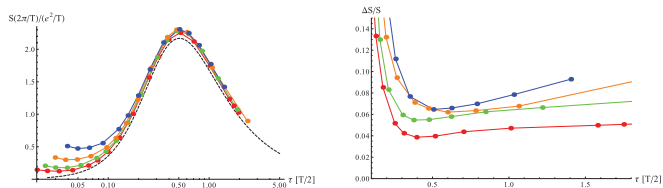


FIG. 10. (Color online) (Left) Same as Fig. 9 for chain lengths  $L = 300, 400, 500$ , and  $600$  (blue, orange, green, and red, or from top to bottom). In each case the period has been chosen as  $T = L/3$ . Smaller chain gives a higher autocorrelation noise. (Right) Relative difference  $\Delta S/S$  between the computed autocorrelation and the theoretical formula, for the same chain lengths, as a function of the escape time from the dot. The relative difference decreases when the chain length (and thus the period  $T$ ) increases; for the longer chain ( $L = 600$ ), the relative difference is about 4%

Moreover, we had to discard the current obtained during the first half-period, as some of its features are different from those of the real periodic current (see the lower right panel of Fig. 8, and the discussion at the end of Sec. III E). Taking  $T = t_{\max}/3 \simeq L/3$  is thus close to the maximum value that can reasonably be taken for the period  $T$ . Another constraint prevents us from taking arbitrarily large values for the escape time. The magnitude of the initial emission time  $t_{in} < 0$  that we need to use increases with  $\tau$ , making it difficult to reach numerically large values of  $\tau$ , as it imposes a larger maximum time  $t_{\max}$ , and thus a longer chain. This is the reason why the largest value of  $\tau/(T/2)$  on Fig. 9 is approximatively 2.

In order to investigate the effects of the finite size on the difference between the numerical results and the theoretical curve, we have computed the current autocorrelation for increasing sizes,  $L = 300, 400$ , and  $500$ , taking  $T = L/3$  in each case. As shown on Fig. 10 (left), taking a smaller chain, and thus a smaller period  $T$ , gives a higher current autocorrelation. We also see that the deviations from the analytical model for large transparencies (bottom left part of the curves) appears for larger values of  $\tau/(T/2)$  for decreasing chain lengths  $L$ . This is because a given value of  $\tau/(T/2)$  corresponds to a larger transparency for a smaller chain, which has a smaller  $T$ .

The right plot of Fig. 10 shows the relative difference between the computed autocorrelation and the theoretical prediction,  $\Delta S/S = [S_{(k,k)}(2\pi/T) - S_{\text{theor}}]/S_{\text{theor}}$ , as a function of the escape time  $\tau$ . We see that this relative difference decreases from the 8%–10% range for a chain with  $L = 300$  and  $T = 100$  to approximatively 4% for the  $L = 600$  chain with  $T = 200$ . One can thus expect that using a longer chain with a larger  $T$  should bring the numerical results closer to the theoretical prediction, although a systematic difference, independent of the chain length, cannot be excluded from our results.

Our simulations allow us to compute easily the autocorrelation noise for different operating regimes, which cannot be described by the semiclassical model. As an example, we have considered the resonant regime, where for the two values of  $V(t)$  there is a dot level resonant with the Fermi energy (see left panel of Fig. 11). This regime is not expected to provide good quality emission of single electrons, as two levels are contributing equally, at the same time, to the electron emission

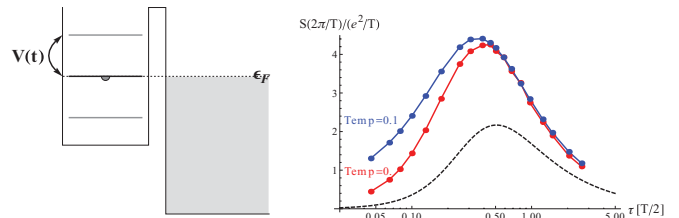


FIG. 11. (Color online) Autocorrelation noise in a same setup as in Fig. 9, in the resonant regime: dot levels are put at the Fermi energy by the external potential (see left panel). The curves with dots show the results obtained at temperature 0 (red) and 0.1 (blue). The black dashed curve is the analytical prediction in the optimal regime. The noise in the resonant regime is much higher than in the optimal regime, showing that the resonant regime is not suitable for single electron emission.

(the level at the Fermi energy, and the level above it). This is clearly visible in the computed autocorrelation noise (right panel of Fig. 11), which is much larger than the noise in the optimal regime. This regime is also much more sensitive to the temperature since a dot level is always at the Fermi energy: for small emission time  $\tau$ , the noise obtained at a temperature of 0.1 is larger than the one at zero temperature.

#### IV. CONCLUSIONS

In this work, we have shown that real-time simulations on a tight-binding chain are a powerful and versatile tool for studying the single-electron emitter, giving the ability to compute accurately elaborate quantities such as the finite-frequency current-autocorrelation noise. Using a noninteracting system, we have shown that the time evolution can be obtained simply and efficiently from the evolution of the one-electron states, and we have derived the formulas for the useful physical quantities (charge on the dot, emitted current, and current autocorrelations) in terms of the numerical object describing the one-electron state's evolution. This allowed us to study the characteristics of the single-electron emitter as a function of different parameters (dot transparency, period of the AC drive, temperature, etc.), giving us access at the same time to illustrative visualizations (current, time-dependent density along the chain, etc.) and providing information about complex quantities. Our calculations of finite-frequency current-autocorrelation noise are in good agreement with theoretical predictions in the regime when these are applicable (and thus also with experimental observations), and can be used to explore other regimes. We have detailed the limitations due to the finite size of the system.

This work can be extended in several directions. First, for noninteracting electrons, we have only explored a small part of the parameter space and of the possible manipulations of the system. We have mainly focused in this work on the optimal regime for single-electron emission as well as the less effective resonant regime, but the method can also be used to study in detail other regimes. We have also limited our study to the case of a perfect piecewise constant time-dependent potential. Our approach can easily be used to study the effect of the experimental limitations on this shape of potential, or to study



different types of potential [for example  $V(t) \sim \sin(t)$ ] that would lead to the emission of electrons with different energy distribution. It also has the ability to simulate a true “one shot” experiment, where a single pulse (rather than a periodic drive) is applied on the dot to emit one electron, starting from an equilibrium situation.

Our method can also be extended to study more elaborate setups based on the manipulation of the emitted single electron. For example, a weak link in the middle of the chain, which would only partially transmit an incoming wave packet, would be equivalent to a quantum point contact. This could be used to perform a real-time study of tomography protocol proposals,<sup>14</sup> or to consider more complex setups such as interferometers.<sup>28</sup> Placing dots at both ends of the chain could also be used to study two-electron interference processes.<sup>29,30</sup>

Second, this work can be seen as a first step toward the study of the single-electron emitter taking into account electronic interactions. As it shows that using a discrete tight-binding model allows us to get a faithful and accurate physical description of the single-electron emitter, we can consider extending our calculations to more powerful methods such as the time-dependent density-matrix renormalization group

(td-DMRG),<sup>16–23</sup> which can include electronic interactions. This work gives us the necessary understanding of the role and limitations of the different parameters in the system (chain size, dot size, period of the AC drive, etc). Using td-DMRG (or similar techniques), we could study the impact on the emitted electron of strong Coulomb interactions inside the dot. We could also consider electronic density-density interactions between two edge states, which should be experimentally relevant, as the experiments have been achieved so far with edge states of the quantum Hall effect with a filling factor  $\nu = 2$ , where two edge states are propagating.

*Note added.* A preprint (Ref. 15) has recently appeared, where details of the Floquet scattering theory for the same setup are presented, together with the semiclassical model.

#### ACKNOWLEDGMENTS

We gratefully acknowledge useful discussions with G. Fève, E. Bocquillon, P. Degiovanni and C. Grenier. This work was supported by the ANR Grant “1 shot” (No. ANR-2010-BLANC-0412).

\*thibaut.jonckheere@cpt.univ-mrs.fr

<sup>1</sup>Mesoscopic Electron Transport, edited by L. L. Sohn, L. P. Kouwenhoven, and G. Schön, NATO Advanced Studies Institute, Series E: Applied Science (Springer, Berlin, 1997), Vol. 345.

<sup>2</sup>Nanophysics: Coherence and Transport, edited by H. Bouchiat, Y. Gefen, S. Gueron, G. Montambaux, and J. Dalibard, École d'Été de Physique des Houches, Session LXXXI (Elsevier, Amsterdam, 2005).

<sup>3</sup>E. Onac, F. Balestro, L. H. Willems van Beveren, U. Hartmann, Y. V. Nazarov, and L. P. Kouwenhoven, *Phys. Rev. Lett.* **96**, 176601 (2006).

<sup>4</sup>E. Zakra-Bajjani, J. Ségala, F. Portier, P. Roche, D. C. Glattli, A. Cavanna, and Y. Jin, *Phys. Rev. Lett.* **99**, 236803 (2007).

<sup>5</sup>R. Aguado and L. P. Kouwenhoven, *Phys. Rev. Lett.* **84**, 1986 (2000).

<sup>6</sup>A. Zazunov, M. Creux, E. Paladino, A. Crépieux, and T. Martin, *Phys. Rev. Lett.* **99**, 066601 (2007).

<sup>7</sup>G. Fève, A. Mahé, J. Berroir, T. Kontos, B. Plaçais, D. C. Glattli, A. Cavanna, B. Etienne, and Y. Jin, *Science* **316**, 1169 (2007).

<sup>8</sup>C. Leicht, P. Mirovsky, B. Kaestner, F. Hohls, V. Kashcheyevs, E. V. Kurganova, U. Zeitler, T. Weimann, K. Pierz, and H. W. Schumacher, *Semicond. Sci. Technol.* **26**, 055010 (2011).

<sup>9</sup>A. Mahé, F. D. Parmentier, E. Bocquillon, J. M. Berroir, D. C. Glattli, T. Kontos, B. Plaçais, G. Fève, A. Cavanna, and Y. Jin, *Phys. Rev. B* **82**, 201309 (2010).

<sup>10</sup>M. Albert, C. Flindt, and M. Büttiker, *Phys. Rev. B* **82**, 041407 (2010).

<sup>11</sup>M. Moskalets and M. Büttiker, *Phys. Rev. B* **66**, 205320 (2002).

<sup>12</sup>M. Moskalets and M. Büttiker, *Phys. Rev. B* **75**, 035315 (2007).

<sup>13</sup>M. Moskalets, P. Samuelsson, and M. Büttiker, *Phys. Rev. Lett.* **100**, 086601 (2008).

<sup>14</sup>C. Grenier, R. Hervé, E. Bocquillon, F. D. Parmentier, B. Plaçais, J. M. Berroir, G. Fève, and P. Degiovanni, *New J. Phys.* **13**, 093007 (2011), ISSN 1367-2630.

<sup>15</sup>F. D. Parmentier, E. Bocquillon, J. M. Berroir, D. C. Glattli, B. Plaçais, G. Fève, M. Albert, C. Flindt, and M. Büttiker, e-print arXiv:1111.3136 (to be published).

<sup>16</sup>S. R. White, *Phys. Rev. Lett.* **69**, 2863 (1992).

<sup>17</sup>M. A. Cazalilla and J. B. Marston, *Phys. Rev. Lett.* **88**, 256403 (2002).

<sup>18</sup>S. R. White and A. E. Feiguin, *Phys. Rev. Lett.* **93**, 076401 (2004).

<sup>19</sup>A. J. Daley, C. Kollath, U. Schollwöck, and G. Vidal, *J. Stat. Mech.* (2004) P04005.

<sup>20</sup>L. G. G. V. Dias da Silva, F. Heidrich-Meisner, A. E. Feiguin, C. A. Busser, G. B. Martins, E. V. Anda, and E. Dagotto, *Phys. Rev. B* **78**, 195317 (2008).

<sup>21</sup>F. Heidrich-Meisner, A. E. Feiguin, and E. Dagotto, *Phys. Rev. B* **79**, 235336 (2009).

<sup>22</sup>A. Branschädel, G. Schneider, and P. Schmitteckert, e-print arXiv:1004.4178 (to be published).

<sup>23</sup>U. Schollwoeck, *Ann. Phys.* **326**, 96 (2011).

<sup>24</sup>A. Branschädel, E. Boulat, H. Saleur, and P. Schmitteckert, *Phys. Rev. B* **82**, 205414 (2010).

<sup>25</sup>J. Bardeen, *Phys. Rev. Lett.* **6**, 57 (1961).

<sup>26</sup>J. Ferrer, A. Martín-Rodero, and F. Flores, *Phys. Rev. B* **38**, 10113 (1988).

<sup>27</sup>J. C. Cuevas, Ph.D. thesis, Universidad Autónoma de Madrid, 1999, Appendix B.

<sup>28</sup>G. Haack, M. Moskalets, J. Splettstoesser, and M. Büttiker, *Phys. Rev. B* **84**, 081303 (2011).

<sup>29</sup>S. Ol'khovskaya, J. Splettstoesser, M. Moskalets, and M. Büttiker, *Phys. Rev. Lett.* **101**, 166802 (2008).

<sup>30</sup>S. Juergens, J. Splettstoesser, and M. Moskalets, *Europhys. Lett.* **96**, 37011 (2011).